ACS Photonics

Article

Cite This: ACS Photonics 2018, 5, 881−889

Lasing Interactions Disclose Hidden Modes of Necklace States in the Anderson Localized Regime

Seung Ho Choi,[†] Kyung Min Byun,[‡] and Young L. Kim*[,†,§]

[†]Weldon School of Biomedical Engineering, Purdue University, West Lafayette, Indiana 47907, United States

[‡]Department of Biomedical Engineering, Kyung Hee University, Yongin 17104, South Korea

[§]Purdue Quantum Center, Purdue University, West Lafayette, Indiana 47907, United States

ABSTRACT: Anderson light localization is known to be minimally affected by nonlinearity (e.g., gain), as a lasing mode typically arises from an isolated localized mode in a passive system. However, in the Anderson localized regime of low-dimensional systems, local resonances can occasionally experience strong level overlap and form an asymmetric single line, which is also known as necklace states. This case is not a hypothetically rare event and indeed is not uncommon. For such passive transport, we experimentally and theoretically investigate how nonlinearity affects necklace states in multilayered systems. When gain or amplifying media are introduced in a system, an asymmetric line splits into multiple lasing peaks, interacting with one another. By decomposing field spectra into a sum of Lorentzian lines, we find that diverging lasing peaks arise from quasimodes; in turn the lifetime and degree of level overlap of the underlying quasimodes are strongly attributed to the threshold and spectral behavior of the emerging lasing modes. These results suggest that observation of lasing interactions could be an alternative yet powerful tool for investigating necklace states (or hybridized states of coupled resonances), the existence of which is challenging to experimentally prove and study, due to grossly single-appearing spectral peaks in passive systems.

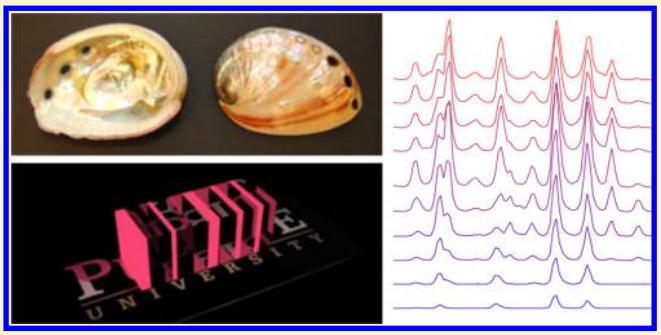

KEYWORDS: *disordered photonics, random lasers, coupled resonances, quasimodes, low-dimensional systems, transfer matrix method, nacre*

In general, lasing modes are considered to represent a subgroup of eigenmodes excited in the localized system.[1−3] A few dominating modes deplete the gain of excited molecules (i.e., gain competition) when the frequencies of the neighboring eigenmodes are very close to one another. In a diffusive regime, multimode lasers exhibit strong modal interactions in the presence of nonlinearity (i.e., gain).[4] In the Anderson localized regime, interference-mediated passive transport without gain can be understood by the degree of level overlap, which is also known as the Thouless number δ for a fundamental localization parameter. Anderson localization supports strong wave confinement with a high quality (Q) factor. Localized modes are sharply divided or isolated in the spectrum with the average spectral space $\Delta\nu$ exceeding the average spectral level width $\delta\nu$: $\delta \equiv \delta\nu/\Delta\nu < 1$. In this case, a localized mode provides such a sharp resonance to induce lasing in gain. Because localized modes are minimally overlapped in frequency and space, modal interactions are known to be suppressed such that a lasing mode grows from a single localized mode of the passive cavity.[5−7]

When $\delta < 1$ in low-dimensional systems (e.g., 2D and 1D), local resonances can occasionally be hybridized in space and frequency and form necklace states, which have a long chain of multiple field peaks in the sample.[8−19] In frequency, necklace states are manifested in the form of a single asymmetric passive line, resulting from strong coupling of spectrally adjacent multiple lines. Importantly, such strong coupling is not a hypothetically rare event.[13] In 1D systems, necklace states have been the object of theoretical investigation[6,8,10−13,18,20−22] as well as experimental studies using disordered multilayered nanostructures found in natural[16,18] and synthetic systems.[11,23] Even in 2D photonic systems, hybridization of local resonances was successfully studied.[14,17,19] Importantly, necklace states are known to play an outsized role in passive transport.[8,10] In the presence of gain, relatively little is, however, known for amplification and lasing of necklace states. Due to the coupled nature of multiple resonances, amplified modes in necklace states could potentially affect one another. Obviously, such a case is contradictory to the notion that Anderson localization suppresses interactions in lasing modes. Thus, it is particularly of interest to investigate lasing interactions within a grossly single-appearing spectral peak of necklace states in passive systems.

For hybridized states of coupled resonances in passive systems, the field intensity spectra can be expressed by a

Received: September 22, 2017
Published: December 20, 2017

DOI: 10.1021/acsphotonics.7b01110
ACS Photonics 2018, 5, 881−889

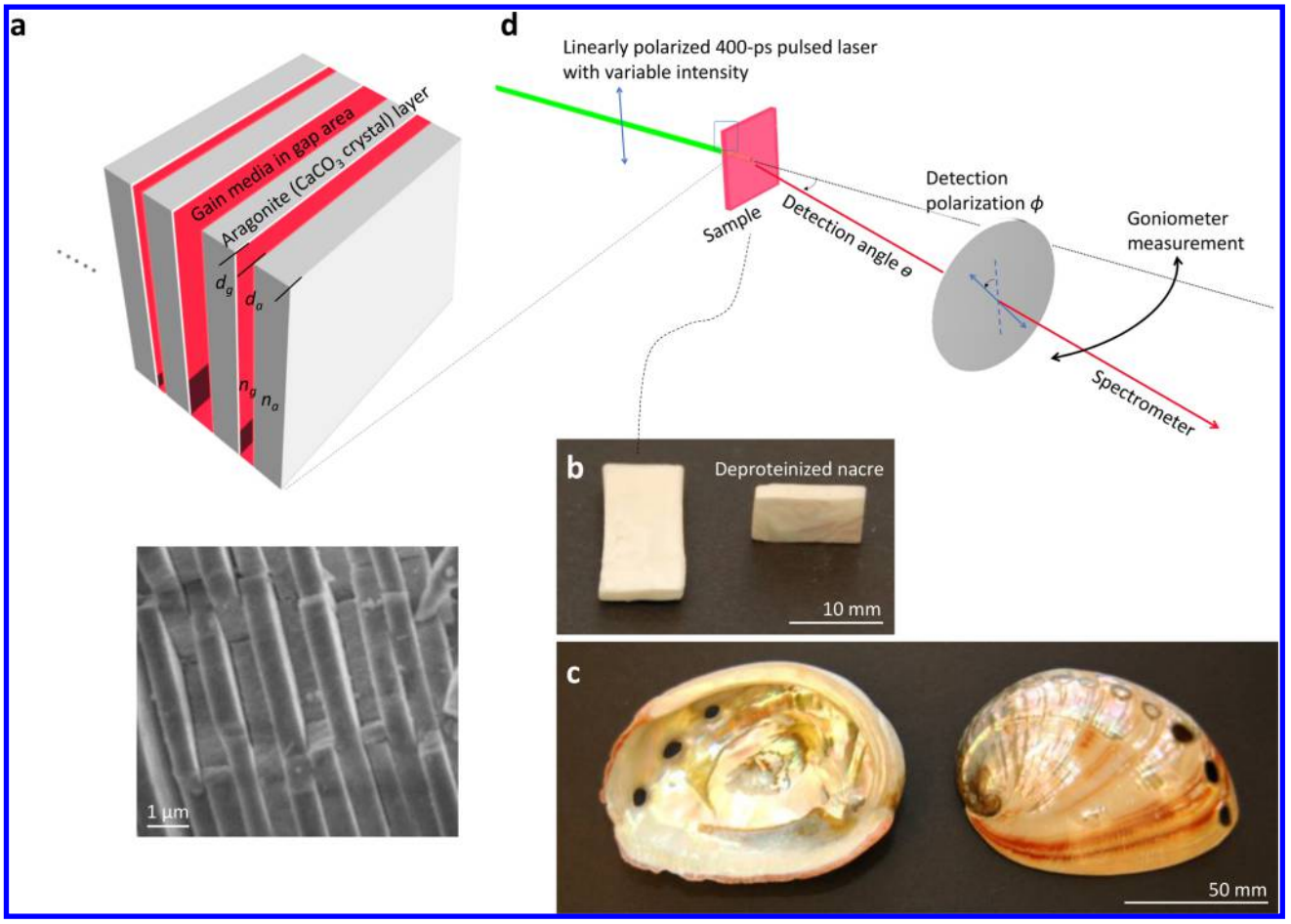

Figure 1. Natural Anderson-localized samples of nacre extracted from abalone shells. (a) Schematic illustration and scanning electron micrograph showing nearly parallel multilayered nanostructures of nacre (mother-of-pearl). (b) Photograph of sliced nacre after removing protein pigments. (c) Photograph of abalone seashells. (d) Schematic illustration of photoluminescent measurements. To excite localized modes in nacre, linearly polarized short pulsed illumination is incident normally on the multilayered nacre structure. The excitation energy is controlled with a linear variable neutral density filter. The lasing emission I_e is characterized in multiple domains of angle, polarization, and spectrum.

superposition of decaying Lorentzian components, which are defined as quasimodes, at each location within a sample.[23,24] The question then arises as to what happens if the underlying quasimodes in necklace states are amplified in the presence of gain. Does one lasing mode arise from the grossly single-appearing peak? Or does one lasing mode correspond to one of the decomposed quasimodes? If so, can the lifetime and degree of level overlap of the underlying quasimodes be correlated with the threshold and spectral behavior of the emerging lasing modes? These questions can be addressed by a modal decomposition analysis, which enables (i) full comparison of the spectral properties of quasimodes (i.e., linewidth and central frequency) with those of lasing modes and (ii) quantification of overlap between quasimodes that leads to spectral repulsion toward the level spacing equilibrium at high excitation energy.

In this Article, we explore interactions of lasing that arise from necklace states in the Anderson localized regime. First, we experimentally demonstrate that spectral variations of lasing modes (e.g., splitting and repulsion) are not uncommon in low-dimensional localized samples. We also characterize the angular and polarization properties of lasing modes and their coupled states. Second, we numerically simulate experimentally observed dynamic responses of lasing modes by introducing the imaginary part of the refractive index of gain media to excitation energy-induced polarization. Third, we computationally extract quasimodes in necklace states by decomposing field spectra into a sum of Lorentzian lines, in which the central frequency and the linewidth are independent from the sample location. This modal decomposition analysis allows us to quantify the lifetime and degree of overlap of underlying quasimodes. As spectral overlap between quasimodes increases, the central frequency of lasing modes is largely shifted, leading to mode repulsion. Moreover, the lifetime of quasimodes obtained from a time−frequency analysis is shown to be strongly correlated with the threshold of emerging lasing modes. Overall, experimental observation and theoretical prediction of lasing properties allow us to better understand the characteristics of necklace states (or coupled resonances), which otherwise would be intrinsically hidden under a grossly single-appearing asymmetric line in a passive system.

Since interference-mediated transport for both classical and nonlinear waves was a challenging theoretical and experimental problem, multilayered structures have widely been used.[6,8,10−13,16,18,20−23,25,26] Nature has many different types of layered nanostructures. For example, nacre (mother-of-pearl) is an immediately exploitable localized sample.[16] The highly multilayered nanostructure of nacre found in nature is beyond synthesized structures using conventional nanofabrication methods. Nacre is composed of microscopic crystals of

DOI: 10.1021/acsphotonics.7b01110
ACS Photonics 2018, 5, 881−889

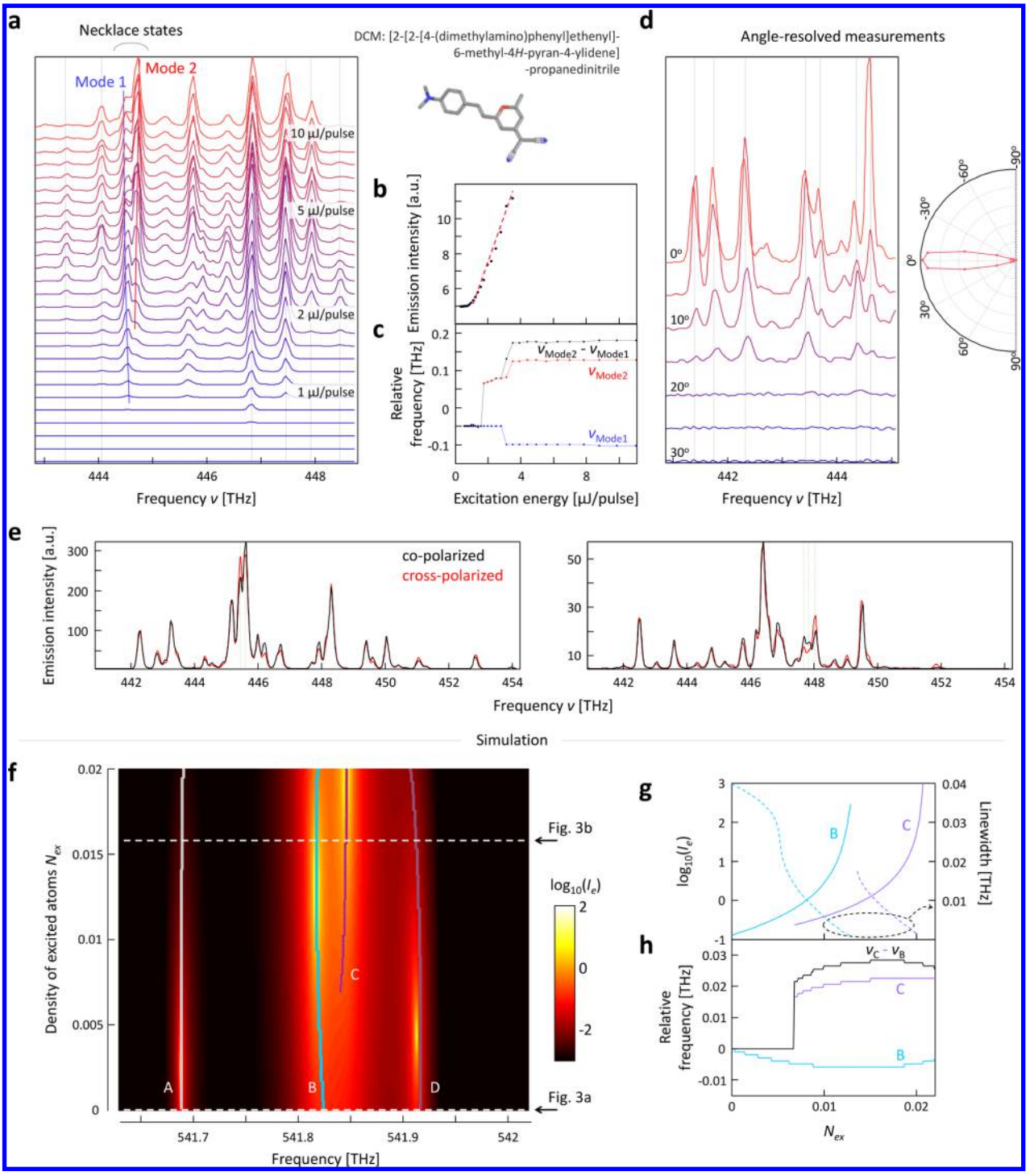

Figure 2. Experimental detection and numerical simulation of lasing mode interactions. (a) Experimental observation of lasing mode variations as the excitation energy E_{ex} increases. The emission spectra are vertically shifted based on a scale of E_{ex}. Inset: Chemical structure of DCM. (b) Measured emission intensity I_e as a function of E_{ex}. (c) Spectral positions of mode 1 and mode 2 marked in (a) and their difference as a function of E_{ex}. (d) Measured emission spectra at different angular directions. The exact forward direction is 0°. Inset: Dependence of the emission intensity on the detection angle. (e) Measured co-polarized and cross-polarized emission spectra at two different locations. The green lines indicate necklace states. (f) Simulation of lasing mode interactions as the density of excited atoms N_{ex} increases. (g) Computed emission intensity I_e and linewidth of mode B and mode C marked in (f) as a function of N_{ex}. (h) Spectral positions of mode B and mode C and their difference as a function of N_{ex}.

calcium carbonate, primarily aragonite (Figure 1a). Specifically, nacre has favorable features for shortening the localization length of light and enhancing the phase randomization as follows: (i) The thickness of the aragonite layer (d_a) is comparable to the wavelength of light, $\lambda \approx 500$ nm. (ii) The variation in d_a is high with a standard deviation of ~10%. (iii) Nacre is composed of a large number of aragonite layers (~4000 layers in a 2 mm nacre sample). (iv) The low structural dimension (i.e., quasi-1D) restricts the volume explored by light waves. Indeed, nacre has inspired a broad range of synthesis and fabrication nanomaterials to mimic its intriguing optical properties.[27]

DOI: 10.1021/acsphotonics.7b01110
ACS Photonics 2018, 5, 881−889

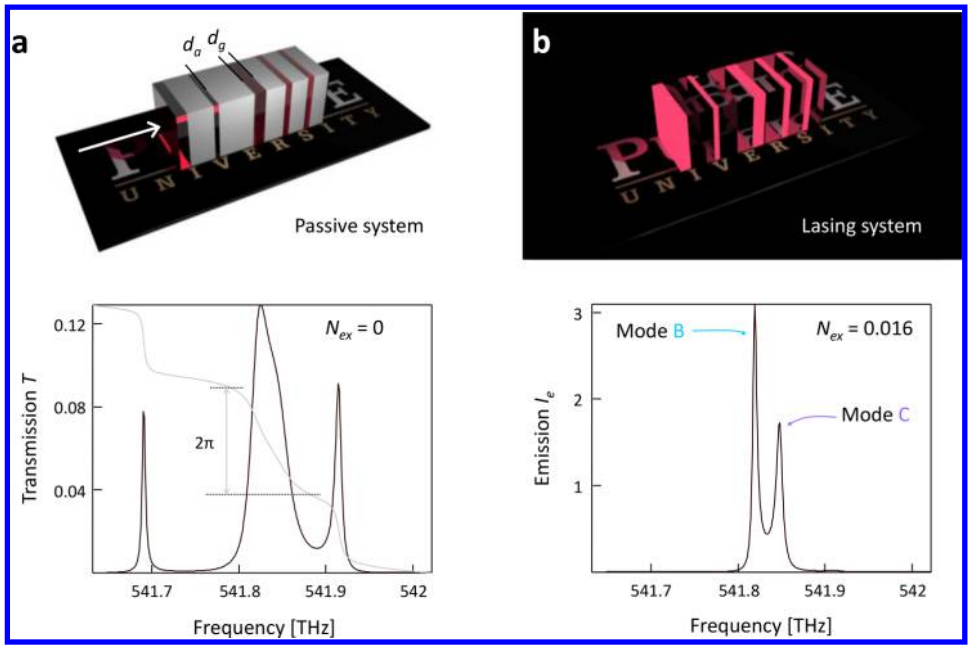

Figure 3. Splitting of an asymmetric single transmission peak into bimodal lasing peaks. (a) Passive transmission T with a peak of asymmetrical shape. T is the field intensity I at the sample output location with $N_{ex} = 0$. The gray line is a phase change in T. (b) Emission intensity I_e growth from T shown in (a). I_e is the field intensity I at the sample output location with $N_{ex} > 0$. N_{ex} used to plot (a) and (b) are marked in Figure 1f.

We experimentally show lasing mode splitting and repulsion from a low-dimensional localized sample (i.e., highly multilayered nanostructures of nacre). A nacre sample is sliced from an abalone shell using a tile saw. To effectively introduce gain, we remove protein pigments that fill the gap between aragonite layers using a sodium hypochlorite (NaOCl) solution (6%). The deproteinization changes the captivating optical reflection of an abalone shell into a bright white color (Figure 1b and c). Then, the deproteinized nacre sample is doped with rhodamine 6G with a concentration of 0.5 mg/mL in methanol or DCM ([2-[2-[4-(dimethylamino)phenyl]ethenyl]-6-methyl-4*H*-pyran-4-ylidene]propanedinitrile) at a concentration of 0.5 mg/mL in dimethyl sulfoxide (DMSO). In particular, DCM in DMSO is useful for obtaining stable lasing emission over a relatively long time (~5 min) to capture the exact dynamics of modes while minimizing any signal artifact and uncertainty. To excite localized modes in nacre, a linearly polarized excitation beam from a frequency-doubled *Q*-switched Nd:YAG laser (pulse repetition rate = 100 Hz, pulse duration = 400 ps, and λ = 532 nm) is incident normally on a 300 μm^2 sample area with a low numerical aperture objective (5×). The excitation beam is spatially fixed on the sample surface, while being focused into a spot with a full width at half-maximum (fwhm) of ~8 μm, avoiding spectral line broadening. In the detection arm (Figure 1d), a polarizer selects the polarization states of lasing emission so that the co-polarized component and the cross-polarized component of the emitted light are recorded independently. In addition, angle-resolved measurements of lasing emission are conducted using a goniometer coupled to a spectrometer with a resolution of ~0.2 nm.

Figure 2a shows lasing spectra from the nacre sample with a thickness of 2 mm. The emission intensity of spectra has clear threshold behavior (Figure 2b). At the lasing threshold, a lasing peak emerges. As the excitation energy further increases, we observe dynamic responses of lasing frequencies (Figure 2c), while generating bimodal lasing peaks from a single lasing peak (i.e., mode splitting) (marked with mode 1 and mode 2 in Figure 2a). In Figure 2d, the lasing emission is highly directional, as nacre is a multilayered nanostructure that restricts the volume explored by light waves into the normal direction of layers. When the input excitation beam is incident normally onto the surface, the effective excitation/amplification of localized modes in nacre can be achieved.[16] Because the transmission and the reflection in nacre closely follow light transport in 1D, the output lasing emission should be highly directional with respect to the incident beam. Thus, angular deviations from the major propagating detection (perpendicular to the layered structures) merely impose a constant prefactor in the emission spectra, while freezing the spectral positions of modes. We note that angle-resolved measurements in disordered systems are not ideal to systematically control or study coupling regimes of modes in a broad spectral range and that temperature tuning or postfabrication methods are often used to modify the dielectric environment of disordered media.[28,29]

In addition, we study the effect of light amplification on polarization in the Anderson localized regime. In Figure 2e, almost all lasing modes are not polarized even with the linearly polarized excitation. Random lasing modes in the strongly scattering regime are known to not be polarization-sensitive, because strong scattering in dye molecules randomizes or scrambles the polarization.[30] On the other hand, we find some bimodal lasing peaks from necklace states are relatively polarization-sensitive. Overall, although the lasing interactions and their polarization states have easily detectable spectral features, it is difficult to resolve the exact spectral profile of necklace states in passive systems due to the limited spectral resolution.

To understand the origin of the diverging lasing peaks and their spectral variations as a function of the excitation energy, we numerically investigate the evolution of optical waves with gain in 1D systems, using the time-independent transfer matrix theory (Methods).[16,18,20,21,31] Mimicking the experimental conditions, we model nanostructures that have 2000 dielectric

DOI: 10.1021/acsphotonics.7b01110
ACS Photonics 2018, 5, 881−889

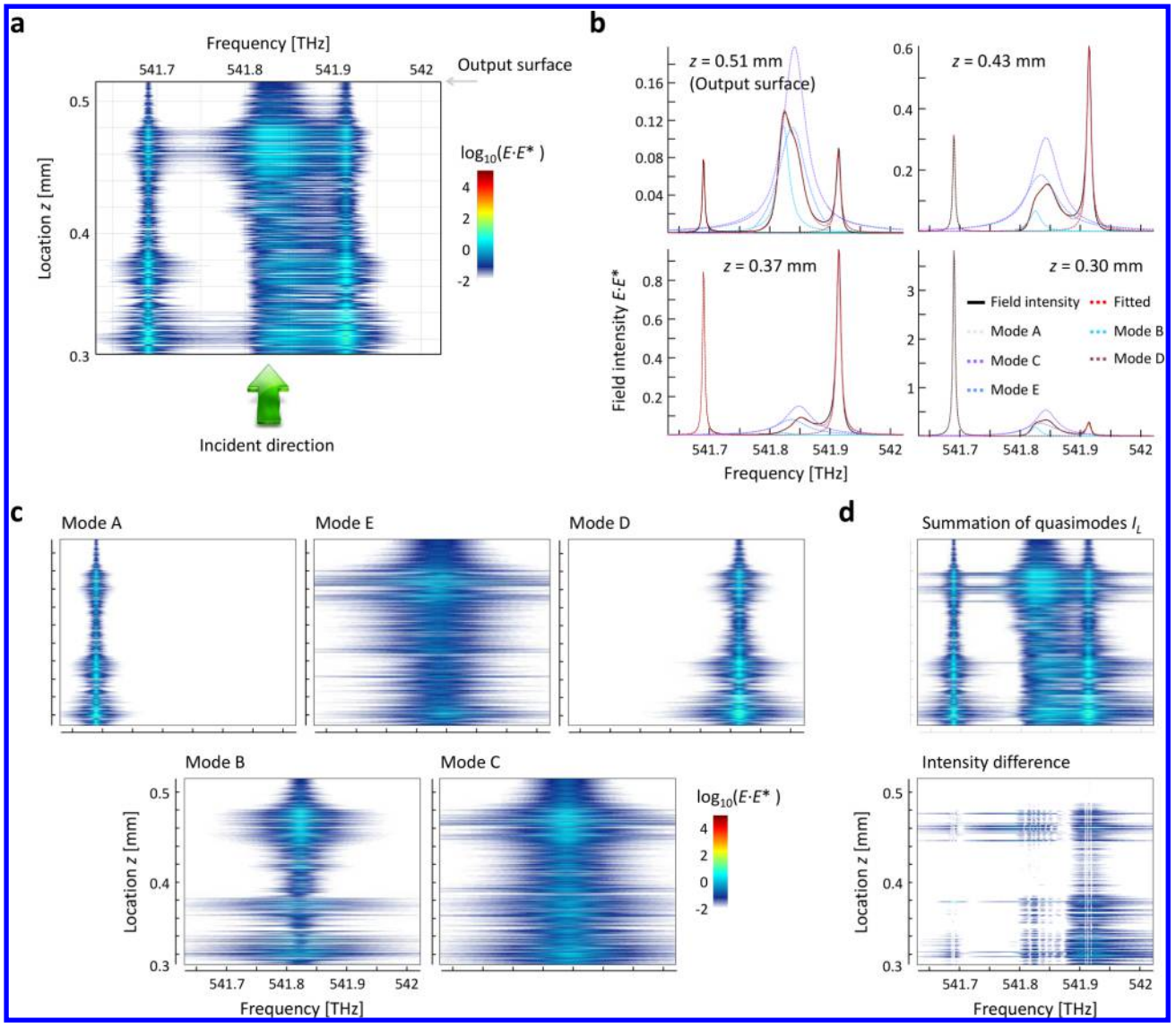

Figure 4. Modal decomposition analysis. (a) Spatial field spectra $I(\nu, z)$ of the passive system with hybridized/coupled states. (b) Comparison of I to Lorentzian terms in eq 1 (i.e., quasimodes A–E) and their summation I_L ($=E_L \cdot E_L^*$) at different locations z. (c) Spatial field spectra of decomposed quasimodes I_n ($=E_n \cdot E_n^*$). (d) Top: I_L summation of five quasimodes in (c). Bottom: Nearly zero difference between I and I_L in the space–frequency domain.

layers with alternating high-index layers $n_a \approx 1.65-1.68$ and lower index gap layers n_g. The thicknesses of aragonite d_a and gap d_g layers are set to be in the ranges of 473 ± 50 nm and 40 ± 10 nm, respectively. Such a disordered system results in a localization length of ∼37.2 μm. This short localization length (≪ total system length of 0.5 mm) ensures that the waves are deeply localized. The gain medium (i.e., rhodamine 6G in methanol) in the gap layers is simulated by adding excitation energy-induced polarization $\chi_g(N_{ex}, \nu)$ to n_g.[20,32]

Figure 2f shows the computed field intensity I ($= E \cdot E^*$) at the sample output surface as a function of excitation energy N_{ex}. In the absence of gain (Figure 3a), the passive transmission T has two narrow peaks of isolated localized modes at ν = 541.69 and 541.92 THz and one relatively broad asymmetric single passive line at ν = 541.83 THz. When N_{ex} = 0.016 (Figure 3b), the single asymmetric line split into two narrow emission peaks I_e and the linewidths of the emerged peaks become narrower than their spectral separation of ∼0.02 THz (Figure 2g). Accounting for the central frequencies of the peaks (Figure 2h), the emerged lasing peaks (blue and purple lines) are largely shifted, compared with the spectrally fixed isolated mode (gray line). As the excitation energy increases, the necklace states show mode competition and repulsion, leading to spectral separation between selected bimodal lasing peaks, while the spectral positions of the isolated lasing modes are frozen. An increase in the excitation energy in the presence of gain (i.e., amplifying medium) can be understood as an increase in the oscillator strength (or Q factor) promoting mode splitting in frequency; the characteristics of optical resonances in disordered media resemble the conventional oscillator.[33] Indeed, this prediction (Figure 2h) is in good agreement with the experimental result of mode splitting (Figure 2c).

From a phase shift of waves, we find a clue for the existence of hybridized/coupled states inside the asymmetric peak. At ν = 541.69 and 541.92 THz in Figure 3a, the transmission of the narrow peaks experiences an accumulated phase shift of π, which is a hallmark of typical isolated localized modes.[12] However, as far as the asymmetric single line is considered, the

DOI: 10.1021/acsphotonics.7b01110
ACS Photonics 2018, 5, 881–889

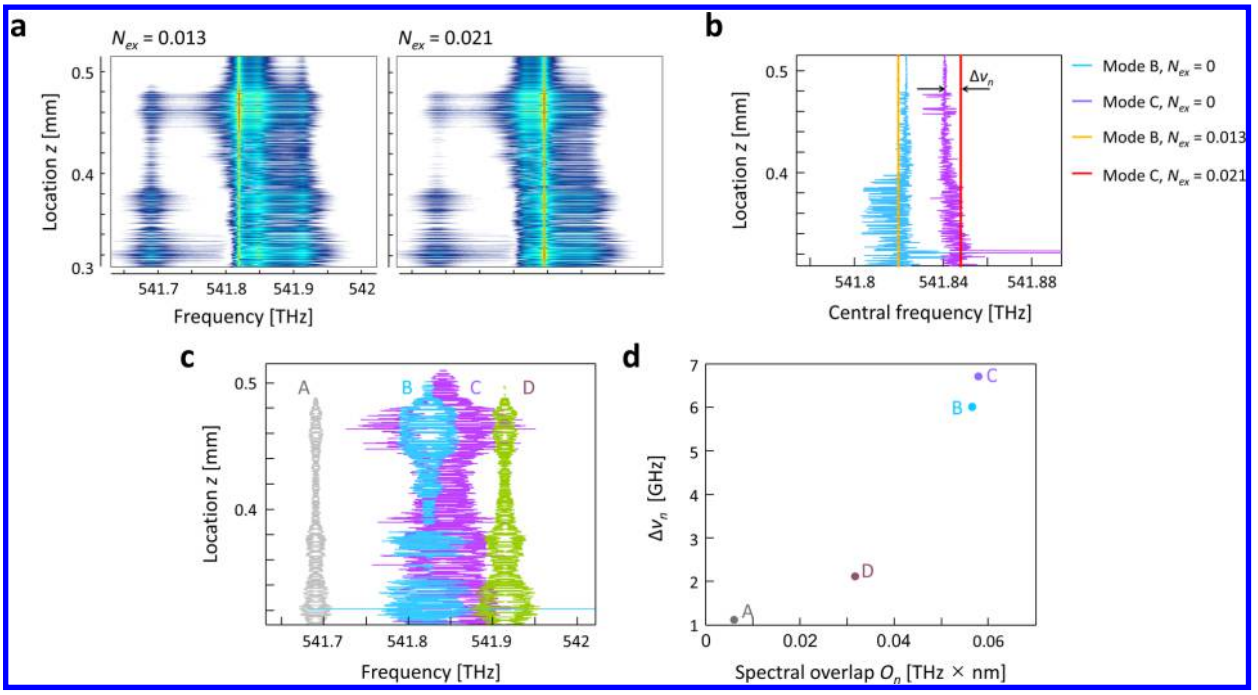

Figure 5. Interplay between spectral overlap of quasimodes and spectral variations of lasing modes. (a) Spatial field spectra $I(\nu, z)$ of the lasing system. The lasing modes, mode B (left) and mode C (right), are excited with different N_{ex}. (b) Central frequencies ν_n of mode B and mode C over locations z in the passive and lasing systems. (c) Borderlines of the spectral extent of quasimodes, with modes A–D demarcated using an intensity cutoff I = 0.2. (d) Spectral shifts of modes $\Delta\nu_n$ as a function of spectral overlap between quasimodes O_n.

phase undergoes a 2π shift between ν = 541.8 and 541.9 THz. Importantly, this indicates that the transport in the asymmetric single passive line is mediated by hybridized states of two possible hidden quasimodes, of which the central frequencies are closely clustered.

To explicitly demonstrate the presence of hybridized states within the asymmetric peak, we conduct a modal decomposition analysis. The field spectrum E at each location z inside the sample is fitted by a sum of Lorentzian lines:[23,24]

$$E_L(\nu, z) = \sum_{n=1}^{N} E_n(\nu, z) = \sum_{n=1}^{N} \frac{A_n(z)}{\Gamma_n(z) + i(\nu - \nu_n(z))} \tag{1}$$

where Γ_n is the linewidth, ν_n is the central frequency of the resonance, $A_n(z)$ is a complex coefficient, and N is the number of quasimodes. N is chosen to be 5 to include isolated modes and slowly varying background. $A_n(z)$, $\Gamma_n(z)$, and $\nu_n(z)$ are inversely found to minimize the objective function F:

$$\min F = \sqrt{\frac{1}{S}\sum_{s=1}^{S}\left|\left| E(\nu_s, z) - \sum_{n=1}^{N} \frac{A_n(x)}{\Gamma_n(z) + i(\nu_s - \nu_n(z))} \right|\right|^2} \tag{2}$$

where ν_s is the sampling frequency at which F is evaluated, $\|\cdots\|$ is the Euclidian norm, and S is the number of ν_s within the frequency of interest. To escape from local minima, we combine stochastic (i.e., genetic algorithm) and deterministic (i.e., Nelder–Mead simplex) optimization methods that use multiple groups of initial guesses.[34]

In Figure 4a, the field spectra of the passive system in the hybridized state include relatively broad spectral peaks inside the sample; the vertical ridges trace the spectral maxima of $I(\nu, z)$. Figure 4b depicts the Lorentzian terms in eq 1, of which the summation fits to the field spectra of Figure 4a at the different locations z inside the sample. As $\Gamma_n(z)$ and $\nu_n(z)$ are specified, each Lorentzian term corresponds to a quasimode. In the range between ν = 541.8 and 541.9 THz, the modal decomposition shows that the two quasimodes (i.e., modes B and C in Figure 4b), the linewidths of which are larger than their spectral separation, mainly contribute to the single asymmetric peak of the hybridized state. We note that mode E is simply the slowly varying background. As shown in Figure 4c, this decomposition is valid for the entire locations z inside the sample. Importantly, the summation of decomposed quasimodes E_L is nearly identical to E (Figure 4d). This result supports the idea that the decomposed quasimodes (Figure 4c) are a complete set of hidden resonances in the asymmetric transmission spectrum. Thus, the set of the hidden quasimodes could potentially mediate the splitting of lasing modes shown in Figure 2f.

In this case, we investigate how the lasing mode behavior is associated with the underlying passive quasimodes. The modal decomposition allows us to characterize a spectral shift $\Delta\nu_n$ between a quasimode and a lasing mode in the hybridized state. Each Lorentzian term in eq 1 is defined by the central frequency ν_n, which is independent over locations with random fluctuations (Figure 5b). When gain is introduced, the fluctuation in ν_n disappears, which in turn sharply defines the lasing mode in the field spectra (Figure 5a). In Figure 5b, the spectral spacing between the lasing modes is larger than that of the quasimodes, resulting in $\Delta\nu_n$ toward the level spacing equilibrium. The quasimodes behave like typical eigenmodes; the quasimodes overlapped in frequency undergo gain competition (i.e., gain depletion) and then repel one another, increasing the frequency spacing between the adjacent lasing modes.

DOI: 10.1021/acsphotonics.7b01110
ACS Photonics 2018, 5, 881–889

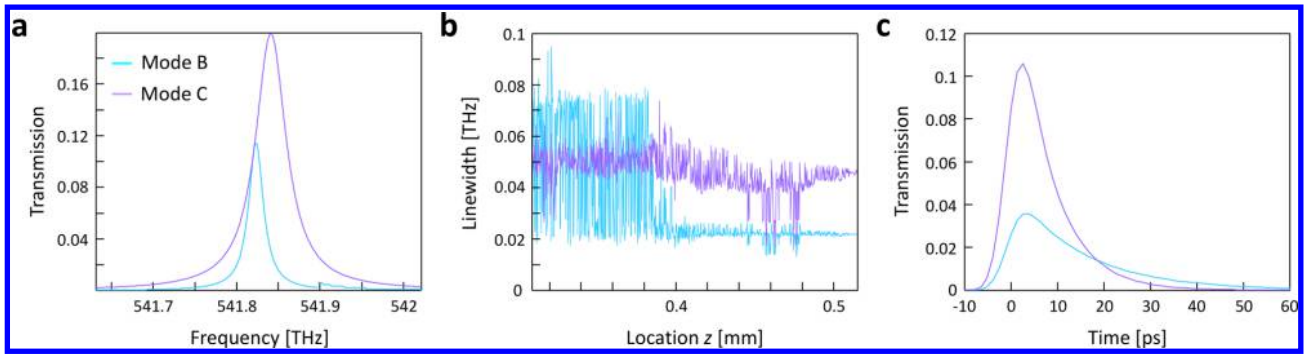

Figure 6. Interplay between quasimode lifetime and lasing threshold. (a) Transmission spectrum of decomposed quasimodes, mode B and mode C, shown in Figure 4b. (b) Linewidths Γ_n of quasimodes, mode B and mode C, over location z. (c) Time-resolved transmission of quasimodes, mode B and mode C, over time with an incident Gaussian pulse of σ_t = 2.5 ps.

To capture the degree of overlapping, we delineate the spectral extent of each quasimode, using an intensity cutoff of ~0.2 (Figure 5c). The borderlines clearly visualize the spectral overlap between the field spectra of the adjacent quasimodes (modes B, C, and D). The spectral overlap varies over z. At the output surface (z = 0.52 mm), the spectral overlap is insignificant. Inside the sample, the spectral overlap is significant through the exponentially falling tails (Figure 5c and c). To quantify the exact degree of overlapping, we calculate an overlapped spectral area of the quasimode O_n with the neighboring quasimodes:

$$O_n = \sum \int_0^{z_0} \int_{-\infty}^{\infty} \min\{I_n(\nu), I_m(\nu)\} \mathrm{d}\nu \, \mathrm{d}z, \text{ for } m \neq n \tag{3}$$

where I_n ($=E_n \cdot E_n^*$) is the field intensity of decomposed modes, I_m is the adjacent quasimodes of I_n, and z_0 is the location of the output surface. As a result, Figure 5d shows the relationship between O_ν and $\Delta\nu_n$. For example, mode C in Figure 5c has the largest calculated overlapping area and the largest $\Delta\nu_n$. This result explains that spectral repulsion becomes stronger as the adjacent quasimodes are closely overlapped. In this nominally localized sample with $\delta < 1$, the interactions of lasing modes increase due to the spectral overlapping of the underlying quasimodes. *Vice versa*, this observation of lasing interactions can be used to qualitatively understand the coupling of quasimodes, which is intrinsically hidden under the asymmetric line of necklace states.

It is also important to predict a mode that will lase first within the overlapped spectrum. For this prediction, we study the lifetime of quasimodes using a time−frequency analysis.[24] In Figure 6a, the decomposed quasimodes at ν = 541.82 and 541.84 THz (i.e., modes B and C) have different linewidths Γ_n, the values of which are relatively consistent over the location z (Figure 6b). By transforming each decomposed quasimode spectrum E_n into the time domain, we obtain a temporal response of each quasimode, which is a pulsed transmission. The pulsed transmission is the Fourier transform of the product of the quasimode spectrum E_n in eq 1 and the Fourier transformed Gaussian pulse E_0:

$$E_0(\nu) \approx \exp\left(-\frac{(\nu - \nu_0)^2}{2\sigma^2}\right) \text{ with } \sigma = \frac{1}{2\pi\sigma_t} \tag{4}$$

where ν_0 is the carrier frequency and σ_t is the Gaussian temporal pulse width. In the time domain, the incident Gaussian pulse is

$$E_0(t, \nu_0) \approx \exp\left(-\frac{t^2}{2\sigma_t^2}\right)\cos(2\pi\nu_0 t) \tag{5}$$

In Figure 6c, the temporal responses are computed from the spectra in Figure 6a with an incident Gaussian pulse of σ_t = 2.5 ps. The decay rates of modes B and C are 16.68 and 8.98 ps^{-1}, which correspond to a Γ_n of 10.7 and 22.2 GHz, respectively. The energy decay of mode B is slower than that of mode C. Thus, this leads mode B to first reach the threshold for lasing in the hybridized state (Figure 2f). Thus, the time−frequency analysis reveals the important role of the lifetime in predicting the underlying quasimodes that are likely to lase. Conversely, the order of the lasing onset provides the information on the lifetime of the underlying quasimode in the passive system.

In conclusion, we report that experimental investigation of lasing interactions can be a useful tool for better understanding Anderson light localization with necklace states in multilayered systems. Spectral profile of necklace states in passive systems is often difficult to resolve and distinguish with isolated localized modes, due to the limited spectral resolution of conventional spectrometers. On the other hand, gain amplifies quasimodes and reveals their characteristics as readily detectable spectral signals of lasing interactions. As lasing modes emerge and grow, multiple quasimodes are decoupled spectrally, which are intrinsically hidden under an asymmetric line of necklace states in a passive system. Through dynamic features in the $\nu - N_{ex}$ domain, we suggest an indirect yet simple approach for experimentally characterizing optical necklace states in Anderson localized systems, without relying on ultrahigh-resolution spectroscopy or time-resolved measurements.

METHODS

Quasimode and Lasing Mode Simulation by Combining Transfer Matrix Method and Semiclassical Laser Theory. To compute quasimodes and lasing modes, we use the transfer matrix method combined with the semiclassical laser theory.[16,18,20,21,31] EM waves (E and H) of a wavenumber k ($= 2\pi/\lambda$) propagating through L_n layers at the normal incidence are described such that

$$\begin{bmatrix} E_1 \\ H_1 \end{bmatrix} = M \begin{bmatrix} E_{L_n+1} \\ H_{L_n+1} \end{bmatrix} = M_1 M_2 \cdots M_L \begin{bmatrix} E_{L_n+1} \\ H_{L_n+1} \end{bmatrix}$$
$$\text{and } M_l = \begin{bmatrix} \cos(kn_l d_l) & i \sin(kn_l d_l)/n_l \\ i \sin(kn_l d_l) n_l & \cos(kn_l d_l) \end{bmatrix} \tag{6}$$

DOI: 10.1021/acsphotonics.7b01110
ACS Photonics 2018, 5, 881−889

where n_l and d_l are the refractive index and thickness of the lth layer, respectively. d_a and d_g fluctuate around 485 and 40 nm, following normal distributions with dispersions s_a and s_g, respectively. Linear gain is implemented by a spatially modulated frequency-dependent susceptibility $\chi_g(z, k)$ in the refractive index of gap area n_g.

$$n_g(z, k) = n_r(z, k) + in_i(z, k) = \sqrt{n_{g(nr)}^2(z, k) + \chi_g(z, k)}$$
$$\text{and } \chi_g(z, k) = \frac{A_m N_{ex}(z)}{k_a^2 - k^2 - ik\Delta k_a} \quad (7)$$

where n_r and n_i (<0) are the real and imaginary parts of the refractive index, $n_{g(nr)}$ is the refractive index of the nonresonant background material, z is the spatial coordinate, A_m is a material-dependent constant, N_{ex} is the density of excited atoms, k_a is the atomic transition frequency (i.e., peak frequency of dye molecules), and Δk_a is the spectral linewidth of the atomic resonance (i.e., spectral width of spontaneous emission of dye molecules).[16] To model rhodamine 6G, k_a = 11.38 μm^{-1} (551 nm) and Δk_a = 0.72 μm^{-1} (35 nm) are used. Both $\mathrm{Re}(\chi_g(k))$ and $\mathrm{Im}(\chi_g(k))$ are proportional to the density of excited atoms N_{ex} determined by the excitation energy. After implementing $n_g(z, k)$ in the characteristic matrix M, the transmission T and the reflectance R can be obtained as follow:

$$T = \frac{2n_0}{n_0 M_{11} + n_0 n_s M_{12} + M_{21} + n_s M_{22}}$$
$$\text{and } R = \frac{n_0 M_{11} + n_0 n_s M_{12} - M_{21} - n_s M_{22}}{n_0 M_{11} + n_0 n_s M_{12} + M_{21} + n_s M_{22}} \quad (8)$$

where n_0 and n_s are the refractive indices of the bottom and top media. For spatial field visualization, the intensity I (= $E \cdot E^*$) is calculated.

AUTHOR INFORMATION

Corresponding Author

*E-mail: youngkim@purdue.edu.

ORCID

Seung Ho Choi: 0000-0002-0365-6422

Young L. Kim: 0000-0003-3796-9643

Notes

The authors declare no competing financial interest.

ACKNOWLEDGMENTS

This work was supported in part by the National Research Foundation of Korea (2017R1A2B4012428), the Kyung Hee University Research Fund in 2015 (KHU-20150800), and the U.S. Air Force Office of Scientific Research (FA2386-17-1-4072).

REFERENCES

(1) Cao, H.; Jiang, X. Y.; Ling, Y.; Xu, J. Y.; Soukoulis, C. M. Mode repulsion and mode coupling in random lasers. *Phys. Rev. B: Condens. Matter Mater. Phys.* **2003**, *67* (16), 161101R.

(2) Jiang, X. Y.; Feng, S. L.; Soukoulis, C. M.; Zi, J.; Joannopoulos, J. D.; Cao, H. Coupling, competition, and stability of modes in random lasers. *Phys. Rev. B: Condens. Matter Mater. Phys.* **2004**, *69* (10), 104202.

(3) Andreasen, J.; Asatryan, A. A.; Botten, L. C.; Byrne, M. A.; Cao, H.; Ge, L.; Labonté, L.; Sebbah, P.; Stone, A. D.; Türeci, H. E.; Vanneste, C. Modes of random lasers. *Adv. Opt. Photonics* **2011**, *3* (1), 88−127.

(4) Tureci, H. E.; Ge, L.; Rotter, S.; Stone, A. D. Strong interactions in multimode random lasers. *Science* **2008**, *320* (5876), 643−646.

(5) Reyes-Gomez, E.; Cavalcanti, S. B.; Oliveira, L. E. Omnidirectional suppression of Anderson localization of light in disordered one-dimensional photonic superlattices. *J. Phys.: Condens. Matter* **2013**, *25* (7), 075901.

(6) Stano, P.; Jacquod, P. Suppression of interactions in multimode random lasers in the Anderson localized regime. *Nat. Photonics* **2013**, *7* (1), 66−71.

(7) Liu, J.; Garcia, P. D.; Ek, S.; Gregersen, N.; Suhr, T.; Schubert, M.; Mork, J.; Stobbe, S.; Lodahl, P. Random nanolasing in the Anderson localized regime. *Nat. Nanotechnol.* **2014**, *9* (4), 285−289.

(8) Pendry, J. B. Quasi-Extended Electron-States in Strongly Disordered Systems. *J. Phys. C: Solid State Phys.* **1987**, *20* (5), 733−742.

(9) Tartakovskii, A. V.; Fistul, M. V.; Raikh, M. E.; Ruzin, I. M. Hopping Conductivity of Metal Semiconductor Metal Contacts. *Soviet Physics Semiconductors-Ussr* **1987**, *21* (4), 370−373.

(10) Pendry, J. B. Symmetry and Transport of Waves in One-Dimensional Disordered-Systems. *Adv. Phys.* **1994**, *43* (4), 461−542.

(11) Bertolotti, J.; Gottardo, S.; Wiersma, D. S.; Ghulinyan, M.; Pavesi, L. Optical necklace states in Anderson localized 1D systems. *Phys. Rev. Lett.* **2005**, *94* (11), 113903.

(12) Ghulinyan, M. Formation of optimal-order necklace modes in one-dimensional random photonic superlattices. *Phys. Rev. A: At., Mol., Opt. Phys.* **2007**, *76* (1), 013822.

(13) Chen, L.; Li, W.; Jiang, X. Y. Occurrence probability and conductance contribution of necklace states: in support of a new scenario of Anderson phase transition. *New J. Phys.* **2011**, *13*, 053046.

(14) Labonte, L.; Vanneste, C.; Sebbah, P. Localized mode hybridization by fine tuning of two-dimensional random media. *Opt. Lett.* **2012**, *37* (11), 1946−1948.

(15) Chen, L.; Jiang, X. Y. Characterization of short necklace states in the logarithmic transmission spectra of localized systems. *J. Phys.: Condens. Matter* **2013**, *25* (17), 175901.

(16) Choi, S. H.; Kim, Y. L. Hybridized/coupled multiple resonances in nacre. *Phys. Rev. B: Condens. Matter Mater. Phys.* **2014**, *89* (3), 035115.

(17) Pena, A.; Girschik, A.; Libisch, F.; Rotter, S.; Chabanov, A. A. The single-channel regime of transport through random media. *Nat. Commun.* **2014**, *5*, 3488.

(18) Choi, S. H.; Byun, K. M.; Kim, Y. L. Excitation of multiple resonances in 1D Anderson localized systems for efficient light amplification. *Opt. Lett.* **2015**, *40* (5), 847−850.

(19) Sgrignuoli, F.; Mazzamuto, G.; Caselli, N.; Intonti, F.; Cataliotti, F. S.; Gurioli, M.; Toninelli, C. Necklace State Hallmark in Disordered 2D Photonic Systems. *ACS Photonics* **2015**, *2* (11), 1636−1643.

(20) Jiang, X. Y.; Soukoulis, C. M. Time dependent theory for random lasers. *Phys. Rev. Lett.* **2000**, *85* (1), 70−73.

(21) Soukoulis, C. M.; Jiang, X. Y.; Xu, J. Y.; Cao, H. Dynamic response and relaxation oscillations in random lasers. *Phys. Rev. B: Condens. Matter Mater. Phys.* **2002**, *65* (4), 041103R.

(22) Sheinfux, H. H.; Kaminer, I.; Plotnik, Y.; Bartal, G.; Segev, M. Subwavelength Multilayer Dielectrics: Ultrasensitive Transmission and Breakdown of Effective-Medium Theory. *Phys. Rev. Lett.* **2014**, *113* (24), 243901.

(23) Sebbah, P.; Hu, B.; Klosner, J. M.; Genack, A. Z. Extended quasimodes within nominally localized random waveguides. *Phys. Rev. Lett.* **2006**, *96* (18), 183902.

(24) Wang, J.; Genack, A. Z. Transport through modes in random media. *Nature* **2011**, *471* (7338), 345−8.

(25) Jordan, T. M.; Partridge, J. C.; Roberts, N. W. Disordered animal multilayer reflectors and the localization of light. *J. R. Soc., Interface* **2014**, *11* (101), 20140948.

(26) Milner, V.; Genack, A. Z. Photon localization laser: Low-threshold lasing in a random amplifying layered medium via wave localization. *Phys. Rev. Lett.* **2005**, *94* (7), 073901.

DOI: 10.1021/acsphotonics.7b01110
ACS Photonics 2018, 5, 881−889

(27) Finnemore, A.; Cunha, P.; Shean, T.; Vignolini, S.; Guldin, S.; Oyen, M.; Steiner, U. Biomimetic layer-by-layer assembly of artificial nacre. *Nat. Commun.* **2012**, *3*, 966.
(28) Garcia, P. D.; Lodahl, P. Physics of Quantum Light Emitters in Disordered Photonic Nanostructures. *Ann. Phys.* **2017**, *529* (8), 1600351.
(29) Riboli, F.; Caselli, N.; Vignolini, S.; Intonti, F.; Vynck, K.; Barthelemy, P.; Gerardino, A.; Balet, L.; Li, L. H.; Fiore, A.; Gurioli, M.; Wiersma, D. S. Engineering of light confinement in strongly scattering disordered media. *Nat. Mater.* **2014**, *13* (7), 720−725.
(30) Knitter, S.; Kues, M.; Haidl, M.; Fallnich, C. Linearly polarized emission from random lasers with anisotropically amplifying media. *Opt. Express* **2013**, *21* (25), 31591−31603.
(31) Xu, Z.; Sun, X.; Liu, J.; Song, Q.; Muckley, M.; Akkus, O.; Kim, Y. L. Spectroscopic visualization of nanoscale deformation in bone: interaction of light with partially disordered nanostructure. *J. Biomed. Opt.* **2010**, *15* (6), 060503.
(32) Andreasen, J.; Vanneste, C.; Ge, L.; Cao, H. Effects of spatially nonuniform gain on lasing modes in weakly scattering random systems. *Phys. Rev. A: At., Mol., Opt. Phys.* **2010**, *81* (4), 043818.
(33) Bliokh, K. Y.; Bliokh, Y. P.; Freilikher, V.; Genack, A. Z.; Sebbah, P. Coupling and level repulsion in the localized regime: From isolated to quasiextended modes. *Phys. Rev. Lett.* **2008**, *101* (13), 133901.
(34) Choi, S. Fast and robust extraction of optical and morphological properties of human skin using a hybrid stochastic-deterministic algorithm: Monte-Carlo simulation study. *Lasers in Medical Science* **2010**, *25* (5), 733−741.

DOI: 10.1021/acsphotonics.7b01110
ACS Photonics 2018, 5, 881−889